



“O/F Shift” in Hybrid Rockets

Arif Karabeyoğlu*

KOÇ University, Istanbul, Turkey, 34450
SPG Inc., Palo Alto, California, 94306

Elena Toson†

Politecnico di Milano, Milano, Italy,

and

Brian Evans‡

Stanford University, Stanford, CA 94305

For most hybrid rocket systems, oxidizer to fuel ratio (*O/F*) changes over time due to 1) natural growth of the fuel port diameter and 2) oxidizer flow rate variations, if throttling is employed. This phenomenon, which is referred to as “*O/F* shift”, leads to a reduction in motor performance. Note that liquid or solid rocket motors are not subject to temporal *O/F* variations, which is wrongfully considered as one of the most critical disadvantages of hybrid rockets. In this paper, the effect of “*O/F* shift” is quantified for hybrid rocket motors. Analytical formulas for the temporal *O/F* variation and the overall *c** efficiency drop associated with the variation has been derived for single circular port motors. It has been shown that for a typical motor, *c** efficiency drop due to *O/F* variation is well below 0.2%, a value which is too small to be measured in an actual motor test. It is also shown that for a wagon wheel type multiport configuration (with triangular ports), efficiency drop is significantly worse than the single circular port case. Even for the multiport systems, the shift does not have a controlling effect on the overall efficiency of the motor. A number of strategies have been outlined to control the adverse effects of *O/F* variation in a hybrid rocket. For a single circular port design with limited throttling, no mitigation is required. For systems with deep throttling requirements, aft oxidizer injection seems like a viable strategy to retain a high level of overall efficiency.

Nomenclature

a	= Regression rate law coefficient
A_n	= Nozzle throat area, m ²
c^*, c^+	= Characteristic velocities, m/s
C_D	= Nozzle discharge coefficient
C_n	= Constant
D	= Port diameter, m
G_{ox}	= Oxidizer mass flux, kg/m ² -s
G_{oxref}	= Reference oxidizer mass flux, kg/m ² -s
K, K_n	= Integration constant
L	= Fuel grain length, m
\dot{m}_f	= Fuel flow rate, kg/s
\dot{m}_{ox}	= Oxidizer flow rate, kg/s

* President & CTO, SPG Inc., Assistant Professor, Mechanical Engineering Department, Associate Fellow AIAA

† Ph.D. Candidate, Aerospace Engineering Department, Via Privata Giuseppe La Masa 34, 20156 Milano, Italy, Member AIAA

‡ Research Associate, Department of Aeronautics and Astronautics, Member AIAA

\dot{m}_{oxaft}	= Aft oxidizer flow rate, kg/s
\dot{m}_{oxfore}	= Fore oxidizer flow rate, kg/s
n	= Regression rate law oxidizer flux exponent
O/F	= Oxidizer to fuel ratio
$(O/F)_{opt}$	= Optimum oxidizer to fuel ratio, constant in time
P_c	= Actual chamber pressure, Pa
P_{ci}	= Ideal chamber pressure, Pa
\dot{r}	= Regression rate, m/s
\dot{r}_i	= Initial regression rate, m/s
R_f	= Fuel final diameter to initial diameter ratio, $R_f = D_f / D_i$
SCP:	= Single Circular Port
t	= Time, s
t_b	= Burn out time, s
TR	= Throttling ratio
VL	= Volumetric loading
η_{shift}	= O/F shift efficiency
ρ	= Fuel density, kg/m ³
Subscript:	
ave	= Average
i	= Initial
f	= Final

I. Introduction

Unlike liquid or solid rocket motors, the oxidizer to fuel ratio (O/F) of a typical hybrid rocket motor changes over time. The shift in O/F is caused by: 1) an increase in the fuel port diameter, and 2) a change in the oxidizer mass flow injection (i.e. during a throttling transient). The so called “ O/F shift” effect results in a suboptimal operation with delivered c^* and I_{sp} performance less than the desired optimal level. Even though the “ O/F shift” and its effect on the motor efficiency is a well known phenomenon, a comprehensive analysis of this important issue does not exist in the open literature.

In this paper we predict the oxidizer to fuel ratio variations for single circular port (SCP) motors using analytical and numerical methods. For circular port geometry, closed form solutions are developed for O/F variation in time and the net drop in c^* efficiency of the motor caused by this variation. Some numerical simulations are also conducted for a characteristic multiport design in order to compare multiport systems to single circular port motors in the context of temporal O/F variation. Finally some strategies are discussed in order to mitigate the effects of O/F shift in hybrids.

All treatments are limited to two dimensional cylindrical port geometries. Complex 3D geometries or axial variations in the port geometry that take place during the course of the burn are not addressed in this paper. For the sake of generality, efficiencies are calculated based on characteristic velocity, c^* , which requires no specific information on the nozzle or the ambient pressure. Using the methodologies described in this paper, I_{sp} based efficiencies can easily be estimated.

II. Single Circular Motor Design

In this section we limit the analysis to single circular port hybrid rocket motors. Due to their simplicity and perfect fuel utilization, SCP motors are key to make hybrids competitive with the existing solid and liquid propulsion systems.

A. “ O/F Shift” Efficiency Due to Port Area Increase

In a CSP motor with constant oxidizer mass flow rate, for all mass flux exponents other than 0.5, the oxidizer to fuel ratio continually shifts during the operation of the motor. The objective of this section is to develop a mathematical formulation to estimate the extent of the “ O/F shift” that a hybrid rocket system endures over its course

of operation and also to derive a comprehensive formula for the reduction (or increase) of the combustion efficiency associated with the shift. For the sake of simplicity, the analysis will be conducted for the single circular port geometry, but the results of this section can easily be generalized to other port geometries and to multi-port configurations. A numerical treatment for multiport systems is given later in this paper. For completeness, the discussions will start with the basic ballistic calculations which are extensively covered in the open literature.

1. *O/F Shift Formula:*

If the spatial variations are ignored, the dynamic equation that governs the variation of the port geometry with time is given by the following expression.

$$\frac{dD}{dt} = 2\dot{r} \quad (1)$$

Here D is the port diameter at time t . For a classical hybrid propellant system that follows the power law type expression for the regression rate ($\dot{r} = a G_{ox}^n$), Eq. 1 takes the following form.

$$\frac{dD}{dt} = 2aG_{ox}^n = \frac{a2^{2n+1}\dot{m}_{ox}^n}{\pi^n D^{2n}} \quad (2)$$

For constant oxidizer flow rate, this ordinary differential equation (ODE) for the port diameter can easily be integrated to determine the well known expression for the time variation of the port diameter.

$$D(t) = \left[D_i^{2n+1} + \frac{(2n+1)a2^{2n+1}\dot{m}_{ox}^n t}{\pi^n} \right]^{1/(2n+1)} \quad (3)$$

Note that the total burn time can be solved from this equation and can be written in terms of the other parameters of the problem as

$$t_b = \frac{(D_f^{2n+1} - D_i^{2n+1})\pi^n}{(2n+1)a2^{2n+1}\dot{m}_{ox}^n} \quad (4)$$

The instantaneous oxidizer to fuel ratio (O/F) of the motor can be calculated using the classical definition

$$\frac{O}{F} \equiv \frac{\dot{m}_{ox}}{\dot{m}_f} = \frac{\dot{m}_{ox}^{1-n} D^{2n-1}}{\rho\pi^{1-n} 2^{2n} a L} \quad (5)$$

With use of chain rule Eqs. 3 and 5 can be combined to obtain the following expression for the temporal derivative of the O/F .

$$\frac{d(O/F)}{dt} = \frac{(2n-1)G_{ox}}{2\rho L} \quad (6)$$

Even though this expression cannot be directly integrated to obtain an explicit formula for the time variation of O/F , it reveals the important scaling behavior for the O/F shift phenomenon. Namely the shift is zero for $n=0.5$ and it increases with increasing n . The high instantaneous oxidizer flux also tends to increase the “ O/F shift”. The fuel grain length has the opposite effect, namely the shift reduces with increasing length.

Using Eq. 5, the initial, final and average O/F can be calculated based on the following expressions.

$$\left(\frac{O}{F} \right)_i = \frac{\dot{m}_{ox}^{1-n} D_i^{2n-1}}{\rho\pi^{1-n} 2^{2n} a L} \quad (7a)$$

$$\left(\frac{O}{F}\right)_f = \left(\frac{O}{F}\right)_i R_f^{2n-1} \quad (7b)$$

$$\left(\frac{O}{F}\right)_{ave} = \frac{\dot{m}_{ox} t_b}{\rho L (\pi/4) (D_f^2 - D_i^2)} = \frac{G_{oxi} t_b}{\rho L} \frac{1}{R_f^2 - 1} \quad (7c)$$

Note that the diameter ratio and volumetric loading are defined as

$$R_f = D_f / D_i \quad \text{and} \quad VL = 1 - 1/R_f^2 \quad (8)$$

The averaging method for the O/F is not uniquely determined due to the nonlinear nature of Eq. 5. However the selected average is the proper one to use, since it corresponds to the ratio of the burned oxidizer to the burned fuel in an actual system. This argument will be reinforced later in this section.

A formula for oxidizer flux can be established from Eq. 5 and can be substituted into Eq. 6 to obtain the following ODE for O/F .

$$\frac{d(O/F)}{dt} = K (O/F)^{2/(1-2n)} \quad (9)$$

Here the integration constant is given by the following formula.

$$K = (2n-1) \left[\frac{(2\rho L)^{2n+1} \pi a^2}{\dot{m}_{ox}} \right]^{1/(1-2n)} \quad (10)$$

Eq. 9 can be integrated by the method of separation of variables to obtain the following time variation for O/F .

$$(O/F) = \left[(O/F)_i^{(2n+1)/(2n-1)} + \frac{2n+1}{2n-1} K t \right]^{(2n-1)/(2n+1)} \quad (11)$$

This equation can be further simplified by noting that

$$K t_b = \frac{2n-1}{2n+1} (O/F)_i^{(2n+1)/(2n-1)} (R_f^{2n+1} - 1). \quad (12)$$

The final result for the O/F shift in terms of normalized variables becomes

$$\frac{(O/F)}{(O/F)_i} = \left[1 + (R_f^{2n+1} - 1) \frac{t}{t_b} \right]^{(2n-1)/(2n+1)}. \quad (13)$$

Eq. 13 can be used to predict the “ O/F shift” for a single circular port hybrid with constant oxidizer flow rate. For an example case with $n=0.62$ and $R_f=2$, the variation of O/F is shown in Figure 1.

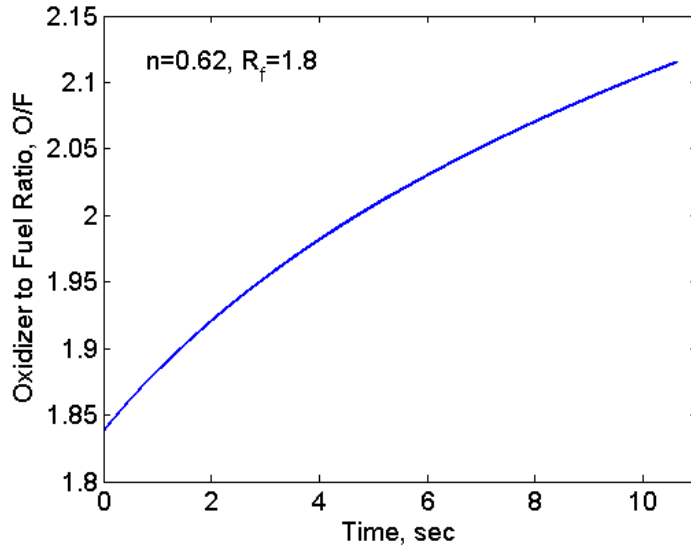


Figure 1. “O/F Shift” as predicted by Eq. 13.

2. *O/F Shift Efficiency Formula:*

The loss of c^* efficiency due to “O/F shift” can be calculated using the c^* equation and the formalism introduced in the previous paragraphs. During quasi-steady state operation of the rocket motor, the mass flow balance at any instant requires that

$$P_c A_n C_d = \dot{m}_{ox} \left(1 + \frac{1}{O/F} \right) c^*(O/F). \quad (14)$$

Over the course of the motor operation this equation can be integrated to result in

$$\int_0^{t_b} P_c A_n C_d dt = \dot{m}_{ox} \int_0^{t_b} \left(1 + \frac{1}{O/F} \right) c^*(O/F) dt = \dot{m}_{ox} \int_0^{t_b} c^+(O/F) dt. \quad (15)$$

The new modified characteristic velocity, $c^+(O/F)$, has been introduced for simplicity.

$$c^+(O/F) \equiv \left(1 + \frac{1}{O/F} \right) c^*(O/F) \quad (16)$$

With use of Eq. 6 time integral can be converted into an integral of O/F .

$$\int_0^{t_b} P_c A_n C_d dt = \frac{\dot{m}_{ox}}{K} \int_{(O/F)_i}^{(O/F)_f} \frac{c^+(O/F)}{(O/F)^{2/(1-2n)}} d(O/F) \quad (17)$$

Note that for given operating conditions and propellants the integral on the right hand side of equation can be numerically evaluated.

The change in efficiency due to the “O/F shift” effect can be calculated relative to an ideal system that operates at a constant oxidizer to fuel ratio which corresponds to $(O/F)_{ave}$ given by Eq. 7c.

$$\int_0^{t_b} P_{ci} A_n C_d dt = \dot{m}_{ox} c^+ [(O/F)_{ave}] t_b \quad (18)$$

The efficiency associated with the time variation of the O/F can be defined as

$$\eta_{shift} \equiv \frac{\int_0^{t_b} P_c A_n C_d dt}{\int_0^{t_b} P_{ci} A_n C_d dt} \quad (19)$$

With use of Eqs. 12, 17 and 18 the efficiency can be written as a function of the known quantities.

$$\eta_{shift} = \frac{(2n+1) \int_{(O/F)_i}^{(O/F)_f} \frac{c^+(O/F)}{(O/F)^{2/(1-2n)}} d(O/F)}{(2n-1)(O/F)_i^{(2n+1)/(2n-1)} (R_f^{2n+1} - 1) c^+ [(O/F)_{ave}]} \quad (20)$$

Here we will outline a procedure that utilizes Eq. 20 to estimate the efficiency drop due to the “ O/F shift” for a hybrid rocket system with constant oxidizer flow rate. The following are the operational parameters selected for the example system: R_f , n , a , \dot{m}_{ox} , ρ , G_{oxi} and $(O/F)_{ave}$.

For these parameters the important variables can be calculated using the following relationships:

$$\text{Initial Diameter: } D_i = \left(\frac{4 \dot{m}_{ox}}{\pi G_{oxi}} \right)^{1/2}$$

$$\text{Final Diameter: } D_f = R_f D_i$$

$$\text{Length: } L = \frac{G_{oxi} t_b}{\rho (O/F)_{ave}} \frac{1}{R_f^2 - 1}$$

Initial and final O/F : Use equations 7a and 7b

The variation of the characteristic velocities with O/F for the LOX/Paraffin-based is shown in Figure 2. Note that the c^* values are calculated using the Air Force Astronautics Laboratory (AFAL) specific impulse (Isp) program. The important observation is that the curves are convex in the range of low O/F and concave for larger O/F .

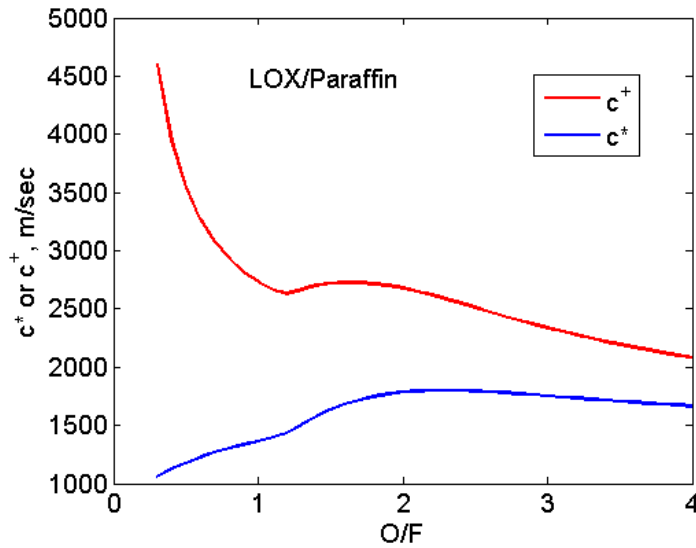


Figure 2. The characteristic velocities c^* and c^+ as a function of O/F for the LOX/Paraffin system. Chamber pressure is 500 psi.

Equation 20 has been used to calculate the efficiencies associated with the “ O/F shift” for the LOX/Paraffin system. The results have been plotted as a function of the average O/F for three values of diameter ratios in Figures 3 and 4 for the mass flux exponents of $n=0.62$ and $n=0.92$, respectively. As shown in Figure 3 the dependency of the shift efficiency on the average O/F is rather complex. Around an average O/F value of 1.2, the efficiency has a sharp peak with peak value higher than 100%. The efficiencies larger than 100% is an artifact of the averaging process and mathematically due to the convex nature of the c^* curve at these low O/F ratios. The other extreme of the efficiency curve is a broad minimum close the optimal O/F value of 2.3 for the LOX/Paraffin system. Efficiency is always less than 100% for the entire O/F domain other than a narrow region in the fuel rich operating regime. The other observation is that efficiency increases towards a value close to 100% with increasing O/F for large O/F . This is due to the almost neutral curvature of the c^* and c^+ curves at large O/F values.

A close examination of the Figures 3 and 4 reveals that the efficiency variation increases with increasing diameter ratio, R_f and the mass flux exponent, n . It is interesting to note that for a typical hybrid system with a diameter ratio of 2 and a mass flux exponent of 0.62 (measured value for the LOX/Paraffin system¹) the efficiency change due to “ O/F shift” is negligible, with a value less than 0.5%. For propellants with larger n exponents the efficiency variation becomes more pronounced. Unless large diameter ratios are employed, the efficiency changes induced by the “ O/F shift” are still small in comparison to the experimental errors in measuring the oxidizer mass flow rate in a hybrid rocket motor.

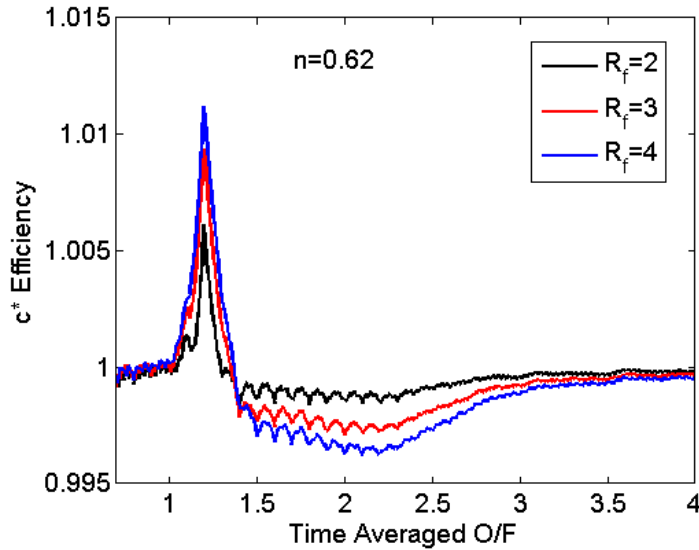


Figure 3. c^* efficiency variation as a function of average oxidizer to fuel ratio for three final to initial port diameter values. The plot is for the LOX/Paraffin system and the mass flux exponent is taken as the experimentally determined value of 0.62.

Shift efficiency variation with average O/F for the N_2O /Paraffin system has been shown in Figure 5. Note that trends are similar to the LOX/Paraffin case with the exception of the stretched O/F scale. Note that the measured n exponent of the N_2O /Paraffin system² is close to 0.5 and thus no efficiency change associated with the “ O/F shift” is expected for this particular propellant combination.

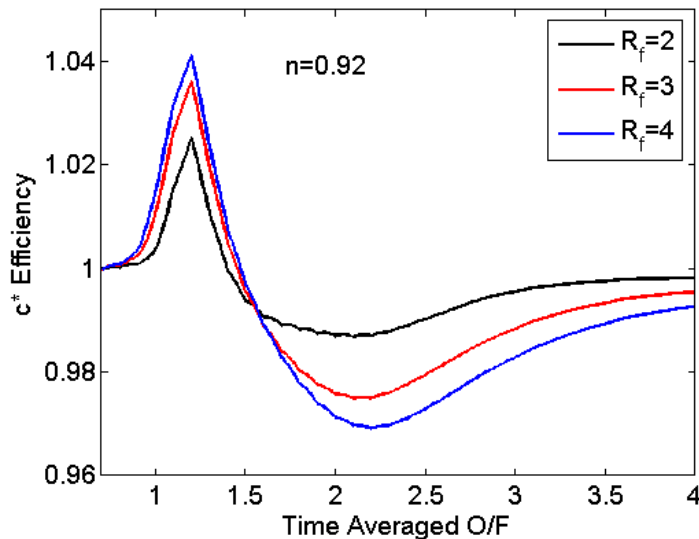


Figure 4. c^* efficiency variation as a function of average oxidizer to fuel ratio for three final to initial port diameter values. The plot is for the LOX/Paraffin system and the mass flux exponent is assumed to be 0.92.

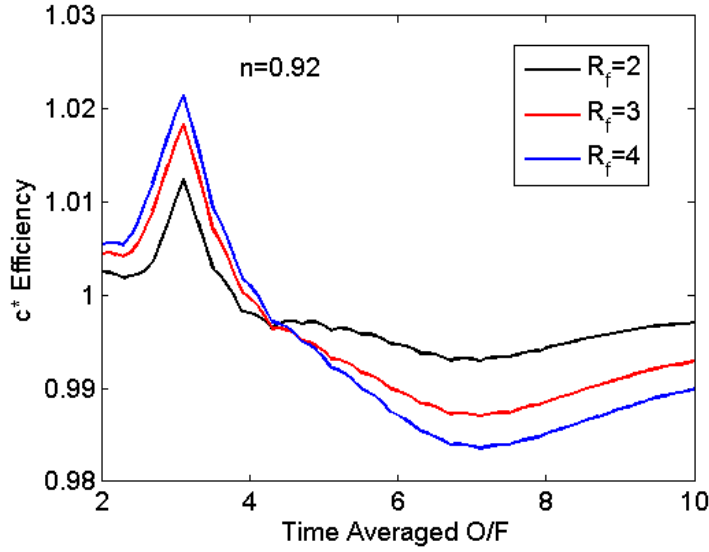


Figure 5. c^* efficiency variation as a function of average oxidizer to fuel ratio for three final to initial port diameter values. The plot is for the N₂O/Paraffin system and the mass flux exponent is assumed to be 0.92.

3. Calculation of the Average Oxidizer to Fuel Ratio:

Based on Eq. 9, the relevant average oxidizer to fuel ratio can be calculated using the following integral expression

$$\frac{1}{(O/F)_{ave}} \int_{(O/F)_i}^{(O/F)_f} \frac{1}{(O/F)^{2/(1-2n)}} d(O/F) = \int_{(O/F)_i}^{(O/F)_f} \frac{(O/F)^{-1}}{(O/F)^{2/(1-2n)}} d(O/F) \quad (21)$$

The integration results in

$$(O/F)_{ave} = \frac{2}{2n+1} \frac{(O/F)_f^{(2n+1)/(2n-1)} - (O/F)_i^{(2n+1)/(2n-1)}}{(O/F)_f^{2/(2n-1)} - (O/F)_i^{2/(2n-1)}} \quad (22)$$

From Eq. 11

$$(O/F)_{ave} = \frac{2}{2n+1} \frac{K t_b}{(O/F)_f^{2/(2n-1)} - (O/F)_i^{2/(2n-1)}} \quad (23)$$

Upon substitution of equations for the initial, final O/F and K into Eq. 23, one can obtain the following simple expression which is equivalent to Eq. 7c.

$$(O/F)_{ave} = \frac{4 \dot{m}_{ox} t_b}{\pi \rho L} \frac{1}{(D_f^2 - D_i^2)} \quad (24)$$

Thus the average used for the O/F is consistent with the mathematically driven average formula.

4. Explanation of the Efficiency Trends:

The dependency of the “*O/F* Shift” efficiency on the average motor *O/F* can be best explained by examining the *c**-*O/F* curves. For the particular case of the LOX/paraffin system, the averaging process is shown in Figures 6 and 7 for the cases of low *O/F* and high *O/F*, respectively. As clearly shown in Figure 6, the averaging process produces a *c** higher than the *c** obtained at the average *O/F* for the motor. This yields efficiencies potentially larger than 100% for motors running under certain fuel rich conditions ($\eta > 1.0$). On the contrary, at high *O/F* values, as shown in Figure 7, the averaged *c** is smaller than the *c** evaluated at the average *O/F*. This means that the efficiency is less than 100% ($\eta < 1.0$).

Based on these arguments, the optimum *O/F* to run a hybrid rocket motor should be based on the following modified optimization which includes the effect of efficiency variation with the *O/F*.

$$\max_{O/F} [\eta_c c_{theo}^* C_F] \quad (25)$$

Note that this modified optimum takes place at a lower *O/F* than the optimum corresponding to the maximum theoretical specific impulse.

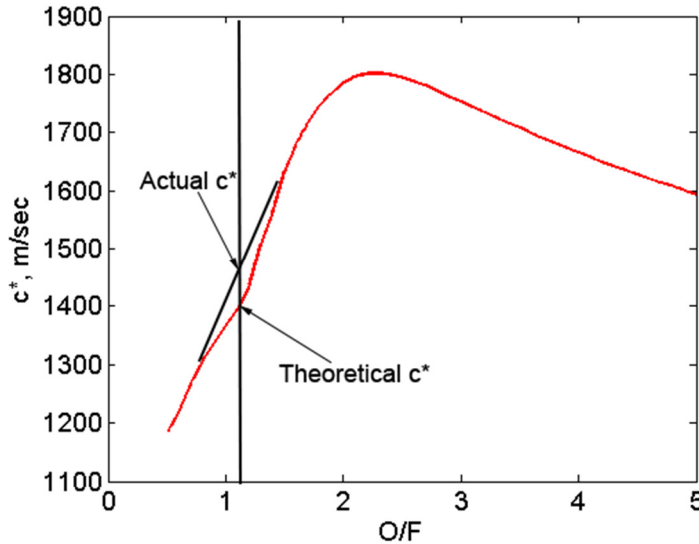


Figure 6. *c**-*O/F* curve for the LOX/paraffin system. Low *O/F* averaging.

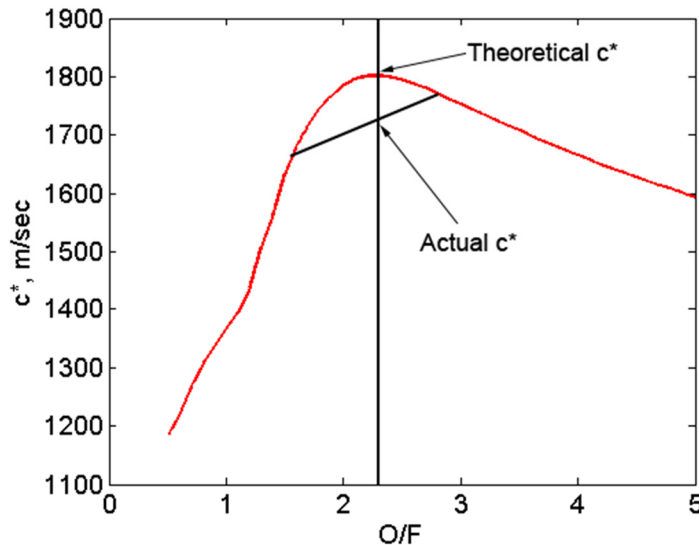


Figure 7. *c**-*O/F* curve for the LOX/paraffin system. High *O/F* averaging.

5. Numerical Calculations for Single Circular Port Design

In order to confirm the analytical results for the single circular port motors derived in the previous section, a numerical simulation study has also been conducted. Port opening and O/F shift effect has been simulated by direct integration of Eq. 2 using the RK4 time marching scheme. All simulation cases assume LOX/paraffin as propellants, average O/F of 3.0, R_f of 2.0 (or VL of 0.75), burn time of 150 s and initial oxidizer mass flux of $220 \text{ kg/m}^2\text{-s}$.

Variation of O/F and c^* with time is shown for various n exponents in Figure 8. As the n exponent is changed, the regression rate coefficient is modified to keep the average regression rate level the same. Note that O/F switches direction at $n=0.5$, the neutral exponent. The shift efficiency over the entire burn is plotted against n exponent in Figure 9. As expected, shift efficiency is 1.0 at $n=0.5$. Efficiency drops slightly as n deviates from 0.5. It is important to note that the efficiency for a typical n value is better than 0.999, indicating a c^* drop less than 0.1% caused by the temporal variation of O/F over the course of the burn. The numerical results are in perfect agreement with the analytical calculations.

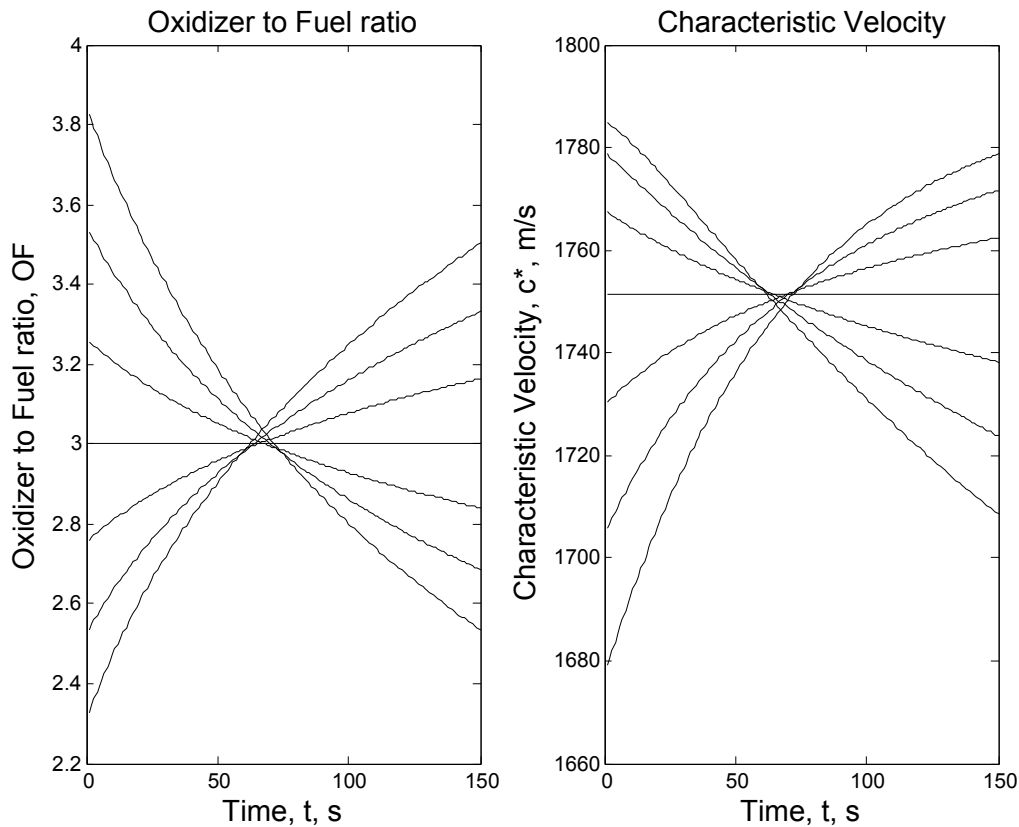


Figure 8. Time variation of O/F and c^* for single circular port motor.

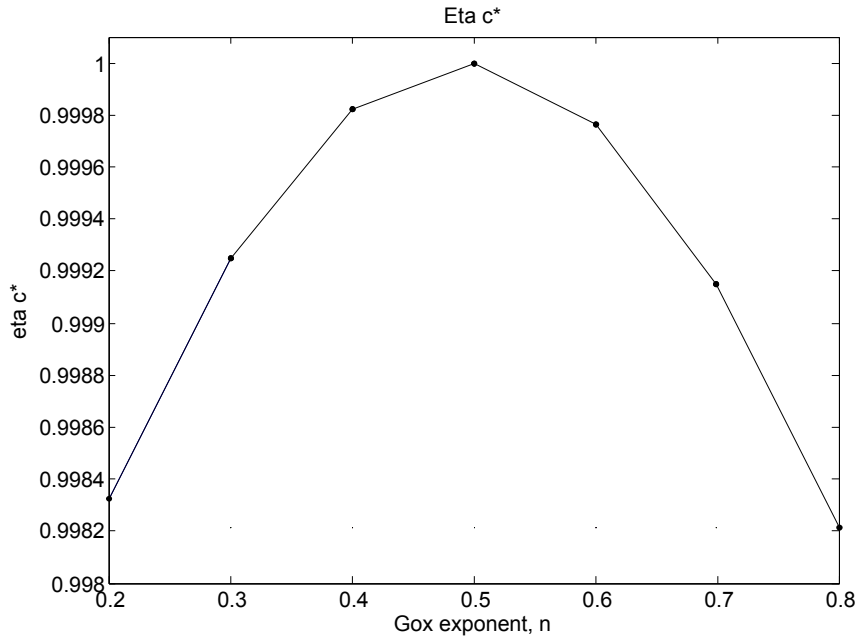


Figure 9. Shift efficiency as a function of oxidizer flux exponent for single circular port motor.

B. Efficiency Due to Throttling

Throttling in a hybrid rocket is achieved by changing the oxidizer mass flow rate that is injected into the motor. Since the fuel mass flow rate is not linearly proportional to oxidizer flow rate for most hybrids, the oxidizer flow rate change induces a shift in the O/F value, which can be predicted using Eq. 5. Unlike the shift due to port opening, shift caused by the throttling action could potentially lead to serious drops in the delivered c^* (and consequently Isp) performance of the motor. The increased sensitivity is primarily due to the fact that oxidizer exponent given in Eq. 5 is typically greater than the diameter exponent. For example for the LOX/paraffin combination ($n=0.62$), effective oxidizer flow rate exponent is 0.38, whereas the diameter exponent is only 0.24. Moreover deep throttling operations lead to significant oxidizer mass flow ratios (as high as 10:1), unlike the port diameter ratios that are typically less than 2.5 for practical systems.

Effect of throttling ratio on the motor efficiency has been calculated for a LOX/paraffin motor operating at an average chamber pressure of 500 psi. We assume that the motor throttles up or down at the midpoint of the burn and stays at the new setting for the duration of the burn. Due to the shallow nature of the c^* curve on the fuel lean side of the O/F range (as shown in Figure 7), we limit the motor operation to this region. Namely for a motor that throttles down, it starts at a point higher than the optimal O/F and finishes at the optimal value. Similarly a motor, which is throttling up, starts at the optimum O/F and finishes its burn at an O/F on the lean side of the optimum. For simplicity, we assume that the throttling ratio is represented by the ratio of the final and initial oxidizer flow rates, $TR = \dot{m}_{oxf} / \dot{m}_{oxi}$. The results for a LOX/paraffin motor are plotted in Figure 10. Note that as n deviates from its neutral value of 1.0, the efficiency drop associated with throttling decreases. For a LOX/paraffin motor with deep throttling such as 10:1, the throttling efficiency can be as low as 0.93. For more reasonable throttling values the efficiency is better than 0.98. In order to control the performance loss of a hybrid operating with high throttling ratios, strategies such as aft oxidizer injection can be implemented. This technique will be discussed in Section IV of this paper. Since the effect of the chamber pressure on c^* is very small, the influence of pressure on the c^* efficiency change can be ignored for most applications.

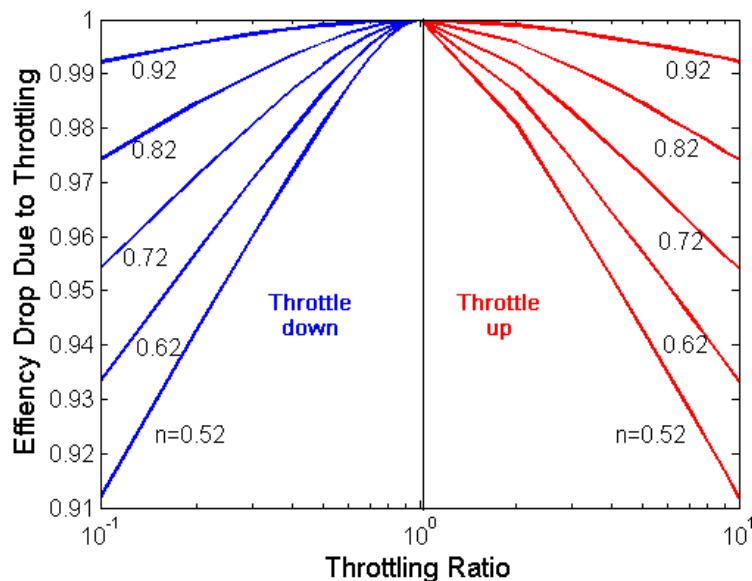


Figure 10. Effect of throttling ratio on the c^* efficiency.

III. Multiport Motor Design

Most practical multiport systems utilize noncircular port shapes in order to minimize the fuel sliver fraction. The time variation for the fuel port perimeter and area for the triangular or trapezoidal geometries that are typically used in the wagon wheel configurations of multiport systems are quite different than the variations experienced by circular port motors. Hence the O/F shift for a multiport system is expected to be different and cannot be predicted by the equations derived in the previous section. Due to the complex nature of the burning geometry and a wide range of port configuration options, no analytical formulas for the multiport systems has been derived. Instead numerical simulations were conducted for a typical wagon wheel design with triangular ports (and a non-burning central circular port) in order to predict the O/F shift and the overall shift efficiency. A schematic for the simulated configuration with 7 burning triangular ports is shown in Figure 11. Port geometry progression is based on Ref. 3.

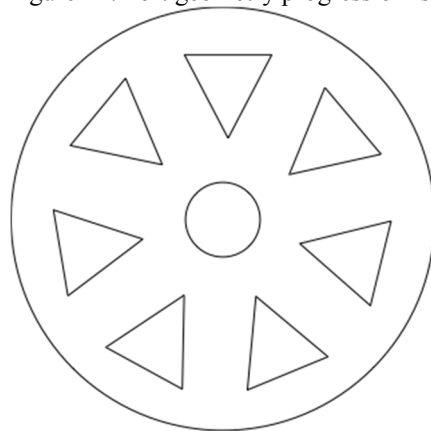


Figure 11. Multiport configuration considered in this study. Center port is not burning. Ports are not equilateral triangles.

Figure 12 shows the results of a simulation with LOX/paraffin type propellants for a volumetric loading of 75%, and an average O/F of 3.0. The oxidizer flux exponent in the regression rate law has been varied from 0.2 to 0.8 by changing the regression rate coefficient a to keep the average regression rate at the same level.

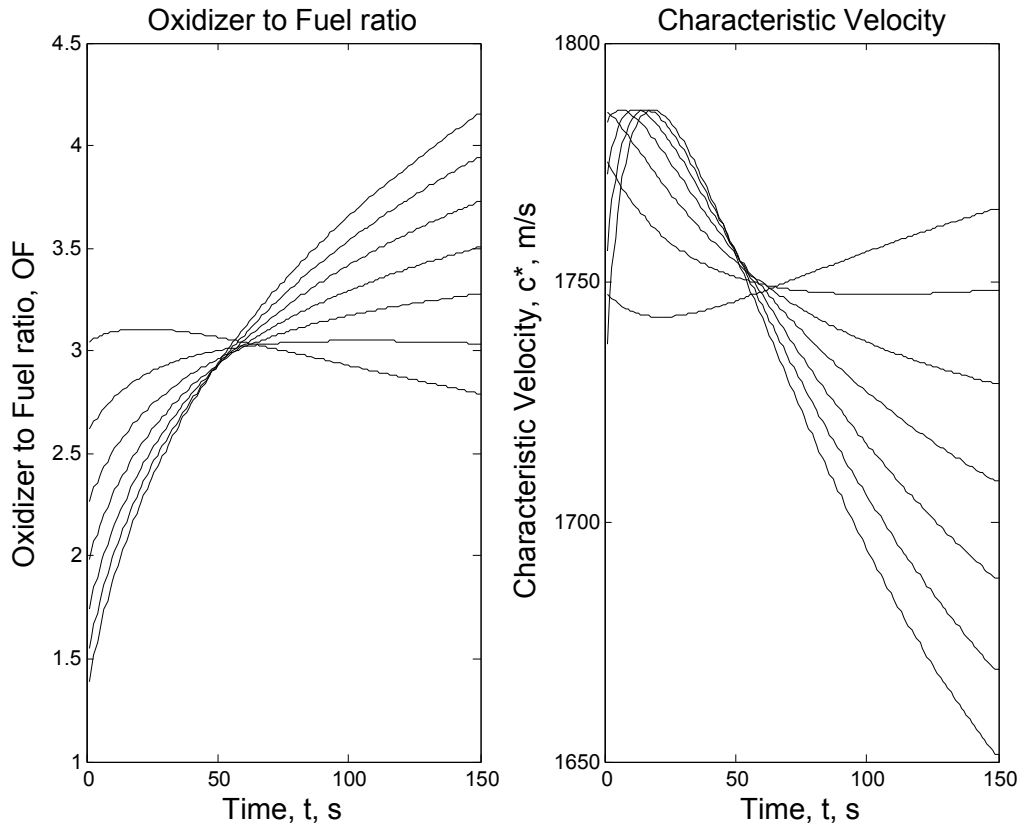


Figure 12. Time variation of O/F and c^* for the multiport configuration shown in Figure 2.

A quick inspection of Figure 12 reveals that, unlike the circular port case, there is no exponent value that leads to a neutral burning. Note that for $n=0.2$ the shift is relatively small, but still finite. The c^* efficiency due to O/F shift is calculated for each n exponent and plotted in Figure 13.

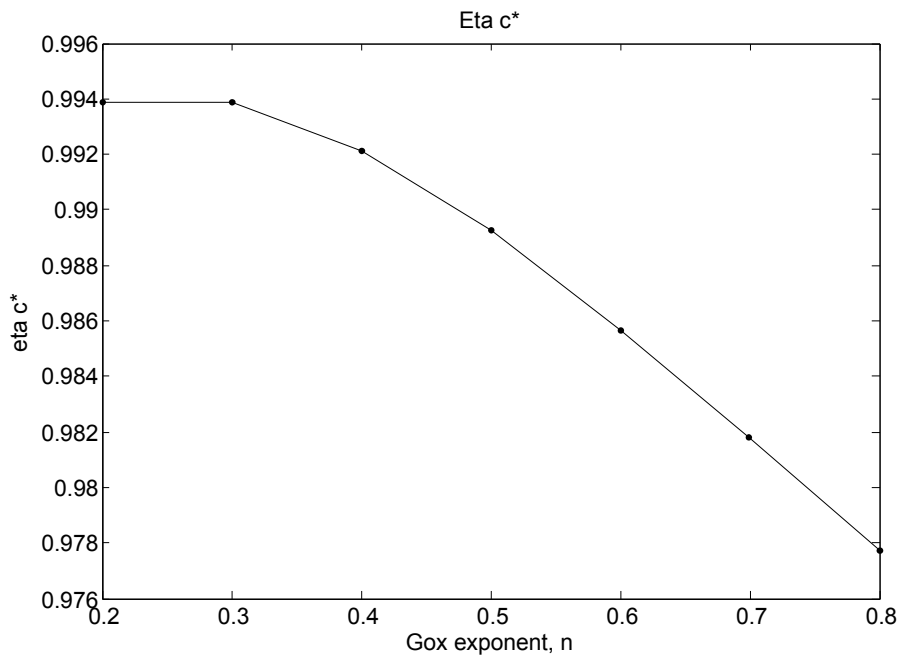


Figure 13. Shift efficiency as a function of oxidizer flux exponent for the multiport configuration.

Note that the efficiency drop for a typical exponent in the 0.6-0.8 range is approximately 2%. This value is much larger than the efficiency drop calculated for a circular port system, which is below 0.1% calculated for the volumetric loading value of 0.75. Thus a wagon wheel system with triangular ports is much more vulnerable to O/F shift effects caused by port opening dynamics. We believe that this conclusion can be generalized to other wagon wheel configurations.

Finally the effect of volumetric loading on the shift efficiency for the multiport system has been investigated and result is shown in Figure 14. It is evident that the efficiency drops almost linearly with volumetric loading, yet the efficiency is quite insensitive to changes in the volumetric loading.

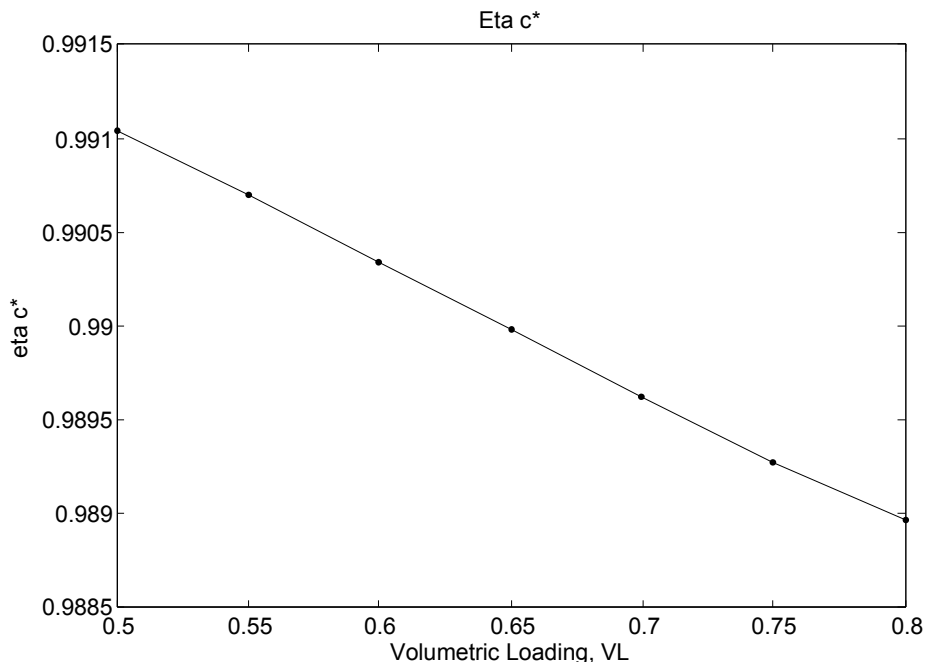


Figure 14. Shift efficiency as a function of volumetric loading for the multiport configuration.

IV. O/F Shift Control

In this section, strategies to control the O/F shift in a hybrid rocket motor will be discussed.

A. Neutral Burning Port Geometries

As discussed previously, circular port geometry does not generate any O/F shift effect for a propellant combination that burns with an n exponent of 0.5. The question whether any other port geometries possess this useful feature can be addressed by investigating the time evolution of the following geometrical grouping for a particular configuration of interest.

$$\frac{O}{F} \propto \frac{A_p^n}{C_p} \quad (26)$$

Here C_p is the circumference of the port and A_p is the port area.

A careful examination of the preceding O/F scaling formula reveals that only regular m -gons (polygon with m vertices), which have m -fold rotational symmetry (equilateral triangle, square regular pentagon etc...), are capable of generating neutral burning for $n=0.5$ (or any other exponent value). The series of m -gons including circle as the limiting case are shown in Figure 15. Note that this feature is only possible if the geometrical similarity is retained during burning. Obviously the only member of this family that could lead to uniform burning around the perimeter is a circle, making it the only practical geometry that can generate neutral burning. Also a nonregular version of any member of this family (such as a rectangle or an ellipse) cannot produce a burn with no shift for any oxidizer flux exponent value.

It can also be shown that, at the same volumetric loading, O/F shift generated (for $n \neq 0.5$) by any of the m -gons are identical. That being said a circular geometry is ideal for eliminating the stress concentration zones and also

for minimizing the residual fuel mass (no corners and perfect matching to pressure vessel geometry). Thus single circular port geometry is by far the best option for a practical system.

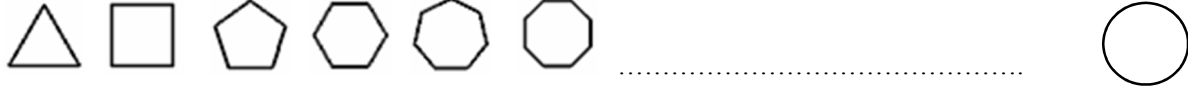


Figure 15. Series of port geometries generating neutral burning for $n=0.5$.

B. Oxidizer Flow Rate Schedule for Neutral Burn (Circular Port)

As can be seen from Eq. 5, O/F shift effect generated by port opening can be completely eliminated by adjusting the oxidizer mass flow rate. For a circular port oxidizer flow rate variation can be written as

$$\dot{m}_{ox} = \left(\frac{C_n (O/F)_{opt}}{D^{2n-1}} \right)^{1/(1-n)} \quad (27)$$

Here $(O/F)_{opt}$ is the selected constant oxidizer to fuel ratio and C_n constant is defined as

$$C_n = a 4^n \pi^{1-n} L \rho \quad (28)$$

Combining Eq. 27 with the dynamic equation for port diameter variation (Eq. 2) yields the following ODE

$$\frac{dD}{dt} = \frac{K_n}{D^{n/(1-n)}} \quad (29)$$

where $K_n = \frac{a 2^{2n+1}}{\pi^n} [C_n (O/F)_{opt}]^{n/(1-n)}$.

Integration and simplification yields the following expressions for port diameter and oxidizer mass flow rate variation for a neutral burn.

$$\frac{D(t)}{D_i} = \left(1 + \frac{2}{1-n} \frac{\dot{r}_i}{D_i} t \right)^{1-n} \quad (30)$$

$$\frac{\dot{m}_{ox}(t)}{\dot{m}_{oxi}} = \left(1 + \frac{2}{1-n} \frac{\dot{r}_i}{D_i} t \right)^{1-2n} \quad (31)$$

Here \dot{r}_i is the initial regression rate of the fuel. The initial oxidizer flow rate is given as

$$\dot{m}_{oxi} = \left(\frac{C_n (O/F)_{opt}}{D_i^{2n-1}} \right)^{n/(1-n)} \quad (32)$$

Note that $\tau_b = \dot{r}_i / D_i$ is the characteristic burning time of the fuel grain. As expected, for $n=0.5$, oxidizer flow variation disappears. Even though this oxidizer flow rate scheduling given by Eq. 31 eliminates O/F shift, it introduces some change in the thrust generated by the motor. It is important to note that, with the single control knob of a classical hybrid (oxidizer valve), both thrust and O/F cannot be controlled simultaneously.

Figure 16 shows the required variation in oxidizer mass flow rate in order to achieve neutral burning. Here the characteristic time, $\tau_b = \dot{r}_i / D_i$ is assumed to be 0.01 sec and the diameter ratio D_f / D_i is 2.0. As expected, increasing n requires more variation in oxidizer flow rate. Even for a low exponent such as 0.62, the required throttle down is substantial, 1.55:1. The small gain in the shift efficiency is not worth the throttling unless the throttling occurs naturally (as in a blow down motor) or is desirable for some reason (such as to minimize axial acceleration).

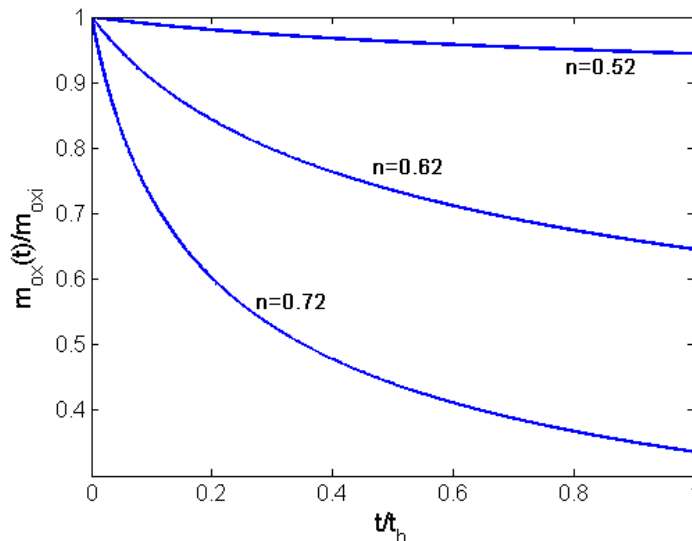


Figure 16. Oxidizer flow rate variation required to achieve neutral burn.

C. Hybrid Rocket with Aft Oxidizer Injection (Circular Port)

The precise and simultaneous control of the thrust force and the I_{sp} for a hybrid system can be achieved by the application of the following methods:

- 1) Introduce radial variation in the fuel formulation to adjust the regression rate such that the O/F shift can be eliminated for a desirable thrust schedule. This is a relatively easy method for fuel systems with adjustable regression rates (such as paraffin-based fuels). However it is a passive method, which requires a precise knowledge of the mission before the motor fabrication.
- 2) Control the regression rate of the fuel by adjusting the swirl number of the injector. An injector for which the total oxidizer flow rate and its angular momentum can be independently adjusted would generate control possibility for thrust and O/F . For the swirl to be effective in controlling the regression rate, the oxidizer needs to be injected in the gaseous phase. This introduces a major complication for practical systems, since the gasification of the liquid oxidizer upstream of the injector poses a significant design challenge.
- 3) Oxidizer can be injected at two locations in the motor: a) Fore end which controls the regression and b) Aft end (behind the fuel grain) such that this portion of the oxidizer does not influence the fuel generation rate. A schematic of such a system is shown in Figure 17. Here we will give a derivation for the aft oxidizer injection schedule for a hybrid motor operating at constant total oxidizer flow rate and O/F (thus constant thrust force). The schedule for a throttling system (for which the total oxidizer flow rate follows a known time variation) can easily be calculated by numerical integration of the dynamic equation.

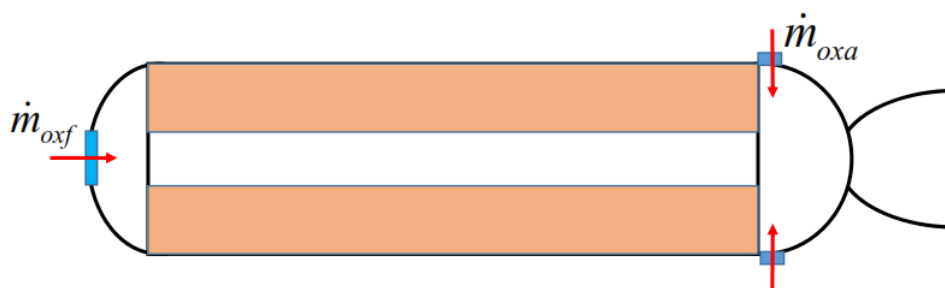


Figure 17. Schematic of a hybrid rocket with aft oxidizer injection.

The O/F ratio expression can be rewritten in terms of fore and aft oxidizer flow rates:

$$C_n(O/F)_{opt} = D^{2n-1} \frac{\dot{m}_{oxfore} + \dot{m}_{oxaft}}{\dot{m}_{oxfore}^n} = D^{2n-1} \frac{\dot{m}_{ox}}{\dot{m}_{oxfore}^n} \quad (33)$$

Combining this expression with the dynamic equation for the port diameter yields the following ODE.

$$D \frac{dD}{dt} = \frac{2a4^n}{\pi^n} \frac{\dot{m}_{ox}}{C_n(O/F)_{opt}} \quad (34)$$

Integration results in the following formula for the port diameter.

$$D(t) = \sqrt{D_i^2 + \frac{a4^{n+1}}{\pi^n} \frac{\dot{m}_{ox}}{C_n(O/F)_{opt}} t} \quad (35)$$

It can be shown that the oxidizer injection schedules can be written as

$$\frac{\dot{m}_{oxfore}(t)}{\dot{m}_{ox}} = \frac{\dot{m}_{ox}^{(1-n)/n} D_i^{(2n-1)/n}}{[C_n(O/F)_{opt}]^{1/n}} \left(1 + \frac{G_{oxref}}{L\rho(O/F)_{opt}} t \right)^{(2n-1)/2n} \quad (36a)$$

and

$$\frac{\dot{m}_{oxaft}(t)}{\dot{m}_{ox}} = 1 - \frac{\dot{m}_{oxfore}(t)}{\dot{m}_{ox}} \quad (36b)$$

Here $G_{oxref} = \frac{4\dot{m}_{ox}}{\pi D_i^2}$ is not a physical oxidizer flux since some of the oxidizer does not flow through the fuel port.

Note that $\tau_s = L\rho(O/F)_{opt} / G_{oxref}$ is the characteristic time scale of the scheduling problem.

V. Conclusions

The following are the grand conclusions for this paper:

- Analytical formulas have been derived for the time variation of O/F and the efficiency reduction associated with the “ O/F shift”. Note that even though these effects are well known, no extensive investigation of the matter exists in the open literature.
- The effect of “ O/F shift” on the c^* efficiency is complicated. For low O/F the efficiencies are higher than 100% due to the convex nature of the c^* curve. For larger O/F the efficiencies are less than 100% (concave c^* curve). Unfortunately the efficiencies take a minimum around optimal O/F . For larger O/F efficiency values increase with increasing O/F .
- For circular port motors, at the mass flux exponent of 0.5, there is no “ O/F shift”. As the n exponent increases from this critical value, the “ O/F shift” and its effect on the efficiency increase dramatically.
- For n exponents associated with paraffin-based fuels (0.5 for N_2O oxidizer and 0.62 for LOX), the efficiency variation associated with “ O/F shift” is negligible. For fuels burning with larger n exponents such as 0.92 and at large diameter ratios (such as 4), the variation in efficiency can be as large as 7% (varies from 104% to 97%).
- The extent of “ O/F shift” and efficiency variation associated with it increases with increasing diameter ratio (or increasing volumetric loading).
- The grand conclusion is that the drop in efficiency due to “ O/F shift” effect inherent to single circular port hybrid rockets is not as large as it is believed in the field. For a typical system with a diameter ratio of 2 and a mass flux exponent of 0.7, the minimum “ O/F shift” efficiency is well over 99%, a drop which is almost impossible to resolve with the accuracy of the commonly used mass flow measurement methods.
- Deep throttling can lead to substantial performance drop in hybrids due to O/F shift effect.
- All regular polygons as fuel port shapes lead to identical O/F shift profiles assuming that they have the same volumetric loading. Regular polygons also lead to neutral burning for $n=0.5$. These statements are only accurate for shapes that retain geometrical similarity as they burn. Thus the only practical shape that satisfies this condition is a circle.

- The efficiency drop associated with typical multiport systems is more substantial than it is with the single circular port systems. Also there is no n exponent that leads to neutral burning for multiport systems.
- Aft oxidizer injection is a viable method to minimize or eliminate the efficiency drop associated with the O/F shift especially for applications requiring deep throttling ratios.

References

¹ M. A. Karabeyoglu, Greg Zilliac, Brian J. Cantwell, Shane DeZilwa and Paul Castellucci “Scale-up Tests of High Regression Rate Paraffin-Based Hybrid Rocket Fuels”, *Journal of Propulsion and Power*, Vol. 20, No. 6, pp. 1037-1045, 2004.

² M. A. Karabeyoglu, “Mixtures of Nitrous Oxide and Oxygen (Nytrox) as Oxidizers for Propulsion and Power Generation Applications”, *Journal of Propulsion and Power*, Vol. 30 , No 3 (2014), pp. 696-706.

³ Humble R. W., G. N. Henry, W. J. Larson, Space Propulsion analysis and design, McGraw-Hill Companies, Incorporated, 1995, pp. 403-442.